Applied Catalysis B: Environmental 330 (2023) 122575

Contents lists available at ScienceDirect

Applied Catalysis B: Environmental

journal homepage: www.elsevier.com/locate/apcatb

Assembly of $ZnZrO_x$ and ZSM-5 on hierarchically porous bio-derived SiO_2 platform as bifunctional catalysts for CO_2 hydrogenation to aromatics

Wen Li [a,c], Guowu Zhan [b,*,1], Xiaobin Liu [c], Yihua Yue [c], Kok Bing Tan [b], Jia Wang [e], Jiale Huang [c,*,2], Qingbiao Li [c,d,**]

[a] College of Advanced Manufacturing, Fuzhou University, 1 Shui Cheng Road, Jinjiang 362200, Fujian, China
[b] College of Chemical Engineering, Huaqiao University, 668 Jimei Blvd, Xiamen 361021, Fujian, China
[c] College of Chemistry and Chemical Engineering, Xiamen University, 422 Siming South Road, Xiamen 361005, Fujian, China
[d] College of Food and Biology Engineering, Jimei University, 185 Yinjiang Road, Xiamen 361021, Fujian, China
[e] College of Chemical Engineering, Nanjing Forestry University, Longpan Road 159, Nanjing 210037, Jiangsu, China

ARTICLE INFO

Keywords:
CO_2 hydrogenation
Bifunctional catalysts
Rice husk
Aromatics
Intimacy criterion

ABSTRACT

Herein, we designed integrated $ZnZrO_x$/ZSM-5 catalysts with adjustable intimacy of the two components for CO_2 hydrogenation to aromatics. The rice husk derived-SiO_2 (denoted as bio-SiO_2) was employed as a platform to tune the intimacy, which can be adjusted by changing the amount of biomass during the catalyst fabrication. It was found that the optimization of intimacy significantly improved the aromatics selectivity from 28% to 74.7%. Importantly, the dimensionless number intimacy was quantified by considering the particle size, density, specific surface areas, and the limiting distance for methanol back-mixing. The intimacy acted as a descriptor governing the aromatics selectivity in the CO_2 hydrogenation reaction, which boosted the transfer and conversion of intermediates from metallic sites to acidic sites. These findings shed light on the understanding of the intimacy criterion for boosting CO_2 hydrogenation to aromatics with the controlled spatial distributions of the two components on a porous bio-platform.

1. Introduction

Direct synthesis of fuels and value-added chemicals from CO_2 hydrogenation has attracted great attention for decreasing CO_2 emissions as well as reducing dependence on petroleum-derived chemicals [1,2]. Aromatics are among the most important bulk chemicals for the production of various polymers with increasing market demand. They are traditionally produced from petroleum cracking or naphtha reforming [3]. Alternatively, aromatics can also be produced through the prospective processes of methanol to aromatics (MTA) and coal pyrolysis [4]. Recently, encouraging progress has been made in converting CO_2 to methanol over diverse metallic (oxides) catalysts, such as ZnO-ZrO_2, Pd/In_2O_3, Pd/Ga_2O_3, In_2O_3/ZrO_2, and so forth [5].

Therefore, the direct conversion of nonpetroleum carbon resources (such as CO_2 or syngas) with green H_2 to aromatics is a promising route to achieve carbon neutrality and reduce the energy crisis [6]. However, the high kinetic reaction barrier and thermodynamic inertness of CO_2 ($\Delta_f G_{298\ K} = -396$ kJ•mol^{-1}) limit its C-C coupling and subsequent conversion to aromatics. Tandem catalytic conversion, which integrates multiple reactions sequentially in a single catalyst under identical conditions, holds great potential to break the equilibrium limitation of CO_2 conversion and enhance product selectivity [7]. For instance, tandem catalysis that integrates the CO_2 hydrogenation to methanol and the MTA processes provides a useful strategy for the selective conversion of CO_2 to aromatics which can break the Anderson-Schulz-Flory (ASF) distribution for Fischer-Tropsch reactions products [8]. Therefore, intensive research and efforts have been devoted to developing high-performance catalysts for CO_2 hydrogenation to value-added aromatics *via* tandem catalysis.

Typically, bifunctional catalysts with metal oxide and zeolite (MO&ZEO) have been extensively studied for CO_2 hydrogenation to aromatics, wherein, the metal oxide (such as $ZnZrO_x$ solid solution) can

* Corresponding authors.
** Corresponding author at: College of Chemistry and Chemical Engineering, Xiamen University, 422 Siming South Road, Xiamen 361005, Fujian, China.
E-mail addresses: gwzhan@hqu.edu.cn (G. Zhan), cola@xmu.edu.cn (J. Huang), kelqb@xmu.edu.cn (Q. Li).
[1] **ORCID** Guowu Zhan: 0000–0002-6337–3758
[2] **ORCID** Jiale Huang: 0000–0001-9069–5739

https://doi.org/10.1016/j.apcatb.2023.122575
Received 16 November 2022; Received in revised form 24 February 2023; Accepted 3 March 2023
Available online 5 March 2023

be used to catalyze methanol formation, and zeolites (such as ZSM-5) can catalyze MTA reactions (*e.g.*, C-C coupling, isomerization, and aromatization reactions) [9]. Therefore, the distinct geometric nature, electronic structure, and diffusion ability of two components in bifunctional catalysts raise the issue of how to combine the two components rationally to maximize their synergy, which has been demonstrated to be crucial for catalytic performance [10]. There are three crucial parameters can be considered for synergy, including the ratio of metal oxide and zeolite, the compatibility of two active sites (*viz.*, properties of zeolites such as topology, acidity strength, density, and hydrogenation ability of the metallic components), and the distance between the two components [11,12].

In particular, the distance between the two components, often described as intimacy (or proximity), which plays a vital role in catalysis, has not been studied in an in-depth manner due to the difficulty in controlling the spatial distribution [13,14]. In a tandem catalysis process, the reaction intermediates should be able to efficiently diffuse from the metal site to the acid sites (referring to the scheme in Fig. S1) [15]. If the distances are too large or the diffusivity is too low, concentration gradients would be developed with a decreased catalytic activity [16]. On the other hand, too close in contact between the metal oxide and zeolite would induce severe metal migration or neutralization of the acid sites of zeolite driven by the harsh reaction conditions, resulting in poor product selectivity [17,18]. However, the quantitative description, as well as which scale of intimacy is more effective in promoting atomization and inhibiting coke deposition, remains unknown.

As for the intimacy criterion, since 1962, when Weisz provided the opinion of "the closer the better", a great number of studies have been focused on putting metal functions as close as possible to the acid sites [19]. However, Zečević et al. have made a breakthrough in the bifunctional catalyst intimacy criterion [20], who reported that Pt metal resides inside the zeolite crystals with the highest possible intimacy to the acid site, which could increase the probability of secondary reactions. Meanwhile, Cheng et al. also discovered that the intimacy effect in the syngas to aromatics tandem reaction was depending on the diffusion of reaction intermediates and the Péclet number (*Pe*) was employed to assess the maximum diffuse distance of methanol intermediates in the catalyst bed [21]. Nevertheless, unraveling the effect of intimacy between two active sites on tandem catalysis performance is still a challenge. The intimacy of metal oxide and zeolite is critical to the efficiency of tandem catalysis. Bio-template with hierarchically porous structures could provide a unique platform to assemble metal oxide and zeolite. Our group has explored diverse bio-templates for the preparation of hierarchically structured nanomaterials, such as pollen [22], rice husk [18], oyster shells[23], *etc*. Therefore, it is possible that MO&ZEO catalysts can also be prepared by integrating metal oxide and zeolite using the natural bio-logical template (*viz.*, rice husk) as a platform. Rice husk is an abundant agricultural by-product (*ca.* 150 million tons/a) [24], which is rich in porous structures (*e.g.*, pores, ridges, tubes) with a high degree of regularity and precise reproducibility [25]. The natural rice husk is rich in silicon (normally more than 88 wt% of SiO_2 in ash), mainly in the form of organically deposited silica hydrate, which can serve as a porous platform. For instance, our group has prepared hierarchically porous ZSM-5 with rice husk as a template to integrate with metal oxide (Pd/ZnO or $ZnZrO_x$) for the direct CO_2 conversion to DME or light olefins [2,18].

Herein, the three-dimensional rice husk and the derived bio-SiO_2 platform provide us with new methods to assemble MO and ZEO components and to investigate the intimacy criterion in CO_2 hydrogenation to aromatics. Recently, our group reported the assembly of distinct zeolites (ZSM-5 and SAPO-34) on the rice-husk-derived platform (bio-SiO_2 platform) [2,26]. The $ZnZrO_x$ solid solution showed super stability and high selectivity for methanol synthesis from CO_2 hydrogenation, with high selectivity of methanol (86%) [27]. In particular, after the combination of the ZSM-5 catalyst, the $ZnZrO_x$&ZSM-5 bifunctional catalyst exhibited outstanding aromatics productivity in the CO_2 hydrogenation reaction [28,29]. In addition, metal-organic frameworks (MOFs) have been exploited as excellent solid precursors and templates for the preparation of integrated nanocatalysts with multicomponent and hierarchical structures, *e.g.*, $ZnZrO_x$ can be prepared by the pyrolysis of Schiff base-modified UiO-66 octahedrons [30]. It is worth noting that the diversity and flexibility of organic ligands in MOFs facilitate the loading of $ZnZrO_x$ on the rice husk matrix.

As can be seen in Scheme 1, we propose to use rice husk as a bio-platform to assemble $ZnZrO_x$ solid solution and ZSM-5 to form a $ZnZrO_x$/ZSM-5 @RH bifunctional catalyst (RH: the rice husk derived bio-SiO_2). $ZnZrO_x$ was first synthesized *in situ* on the surface of a rice husk bio-template to form ZnZrMOF@RH hybrids, wherein, the ZnZrMOF was the precursor of $ZnZrO_x$ [30]. Next, the ZSM-5 precursor was introduced into the ZnZrMOF@RH hybrid suspension to enable the self-assembly of ZSM-5 particles onto the same bio-SiO_2 platform. During the hydrothermal reaction process, ZSM-5 particles could be selectively located in the interstitial space between ZnZrMOF particles which were organized into three-dimension multiscale networks according to the rice husk matrix. Since the bio-SiO_2 is used as a separator to separate $ZnZrO_x$ and ZSM-5 components, tuning the amount of rice husk could lead to different intimacy of the two components. Moreover, the employed bio-SiO_2 as a platform offers the hierarchical porous structure of the resultant MO&ZEO catalysts. Next, the effect of intimacy between the two components on the aromatics selectivity in CO_2 hydrogenation was systematically studied.

2. Experimental section

2.1. Materials

The following chemicals were used without further purification. Zirconium nitrate pentahydrate ($Zr(NO_3)_4{\cdot}5\ H_2O$, ≥ 99.0%), zinc nitrate hexahydrate ($Zn(NO_3)_2{\cdot}6\ H_2O$, ≥ 99.0%), 2-aminoterephthalic acid ($H_2BDC\text{-}NH_2$, ≥99.0%), acetic acid (CH_3COOH, ≥99.5%), N, N-dimethylformamide (DMF, ≥99.5%), sodium aluminate ($NaAlO_2$, 99.5%), salicylaldehyde (≥98%), ethanol (≥99.7%), tetrapropylammonium hydroxide (TPAOH, 25%), tetraethyl orthosilicate (TEOS, 98%) and CD_3OD (AR, 99.8% atom %D) were purchased from Sinopharm Chemical Reagent Co. Ltd. Commercial raw rice husks were bought from a farm in Xiamen (China), and the chemical composition of which can be found in Table S1. The nature rice husk was rich in Si (SiO_2: 29.26 wt%). In particular, by calcination treatment at 550 ℃ to remove the organic matter, the main chemical composition of the bio-SiO_2 platform was mainly 88.02 wt% of SiO_2, 6.68 wt% of K_2O, 0.91 wt % of CaO, 0.1 wt% of MnO, 0.13 wt% of Fe_2O_3, and 0.05 wt% of ZnO. It should be noted that those trace metallic elements would be largely removed during the catalyst fabrication procedure (*vide infra*). First, rice husks were washed thoroughly with distilled water to remove surface dust, and then dried at 80 °C overnight, and stored in a dryer for subsequent use.

2.2. Preparation of ZnZrMOF@RH

In a typical experiment, 0.6 mmol of $Zr(NO_3)_4$ and 0.6 mmol of $H_2BDC\text{-}NH_2$ were added into a mixed solvent of 60 mL of DMF and 4 mL of acetic acid. Next, the desired amount of rice husk (1, 1.5, 2, 2.5, or 3 g) was added and stirred for 5 min. The mixture was then transferred into a Teflon-lined autoclave (volume of 100 mL) for heating at 120 °C for 12 h. The obtained product (denoted as UiO-66-NH_2 @RH) was thoroughly washed with copious amounts of water and then dried at 90 °C overnight. Later, the UiO-66-NH_2 @RH was post-modified by the Schiff base and chelated the zinc ions to form UiO-66-NH_2-SB@RH hybrids based on our previous work [30]. UiO-66-NH_2-SB@RH was dispersed in 30 mL of ethanol under ultrasonication and stirred vigorously. Next, 400 μL of salicylaldehyde and 0.15 mmol of Zn $(NO_3)_2{\cdot}6\ H_2O$ were dissolved in 15 mL of ethanol. After that, the

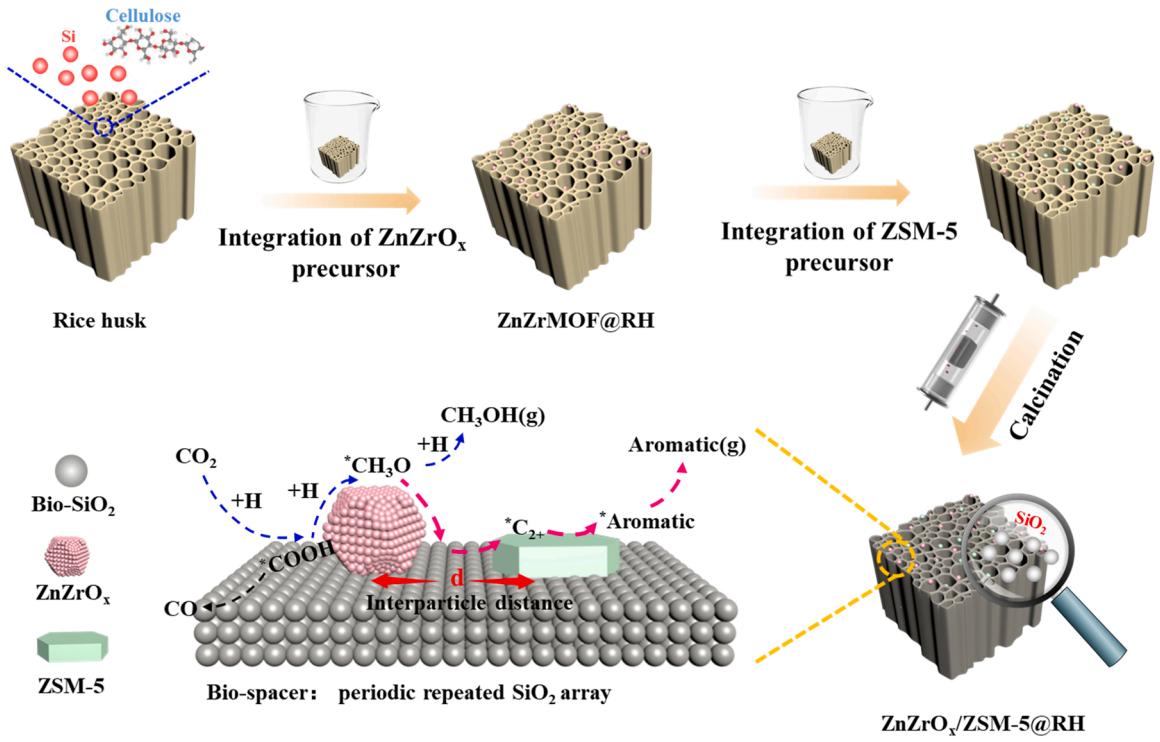

Scheme 1. Schematic illustrations for the synthesis of integrated $ZnZrO_x$/ZSM-5 @RH bifunctional catalysts using bio-derived SiO_2 as a platform (or separator), note: bio-derived SiO_2 was obtained by calcination of rice husk in air atmosphere.

mixture was stirred for 6 h, and was recovered by centrifugation, washed with excess distilled water three times, and dried at 80 °C to obtain the UiO-66-NH_2-SB-Zn@RH product (*i.e.*, the ZnZrMOF@RH).

2.3. Preparation of $ZnZrO_x$/ZSM-5 @RH catalysts

For the preparation of $ZnZrO_x$/ZSM-5 @RH, 2.5 g of TEOS, 9.8 g of $NaAlO_2$ aqueous solution (0.061 mol/L), and 38.4 g of TPAOH (11.6 wt %) aqueous solution were mixed uniformly, and the above-dried ZnZrMOF@RH was added. The mixture was stirred at room temperature for 12 h and transferred to a Teflon-lined autoclave for zeolite crystallization at 170 °C for 12 h. The obtained product was collected by centrifugation, washed with excess water, and dried. Next, the dried sample was calcined at 550 °C for 5 h with a heating rate of 3 °C/min to remove the bio-components and obtain the $ZnZrO_x$/ZSM-5 @RH product. By altering the amount of rice husk, a series of integrated $ZnZrO_x$/ZSM-5 @RH catalysts with distinct intimacy levels of $ZnZrO_x$ and ZSM-5 were synthesized, which were named as $ZnZrO_x$/ZSM-5 @RH-x, *x* represents the amount of rice husk. Besides, to convert the Na-type ZSM-5 to H-ZSM-5, the calcined $ZnZrO_x$/ZSM-5 @RH was ion-exchanged (three times) with 1 mol/L NH_4NO_3 aqueous solution at 80 °C for 1 h, and the product was subsequently calcined at 550 °C for 3 h. Unless otherwise specified, $ZnZrO_x$/ZSM-5 @RH mentioned in the following sections represents the calcined $ZnZrO_x$/H-ZSM-5 @RH. Additionally, since the $ZnZrO_x$/ZSM-5 @RH catalysts were prepared by consecutive hydrothermal, washing, and calcination treatments, the contents of K, Ca Mn, and Fe elements are extremely low in the resultant $ZnZrO_x$/ZSM-5 @RH catalysts (see Table S2), which exclude the effect of these elements on the catalytic performance.

2.4. Catalytic performance evaluation method

As the $ZnZrO_x$/ZSM-5 @RH catalysts with different proximity had different loading contents of the active components, different amounts of $ZnZrO_x$/ZSM-5 @RH were loaded for the evaluation of the catalytic performance to keep the same amounts of active components ($ZnZrO_x$/ZSM-5). It should be noted that the bio-SiO_2 is inert to the CO_2 hydrogenation reaction. Specifically, the reaction of CO_2 hydrogenation to aromatics was carried in a fixed-bed continuous flow reactor loaded with the designed bifunctional catalysts under fixed reaction conditions (340 °C, 3 MPa, $V(H_2)/V(CO_2)/V(N_2)= 72/24/4\%$, and GHSV= 15000 mL/g•h, in terms of the total mass of metal oxide and zeolites (excluding the mass of bio-SiO_2). The product was analyzed online by a gas chromatograph (GC). Plot. Q and WAXMS capillary columns connected to two flame ionization detectors were used to analyze C_1-C_{5+} hydrocarbons and C_6-C_{9+} aromatics, respectively. Other gas products such as CO and CO_2 were separated by a TDX-01 packed column and detected by a thermal conductivity detector. The CO_2 conversion and the selectivity of carbon-containing products, including CO and hydrocarbon products were calculated using Eqs. 1 to 3 with an internal normalization method. The product selectivity is calculated based on molar fractions with carbon basis.

$$CO_2\text{conversion}(\%) = \frac{CO_{2in} - CO_{2out}}{CO_{2in}} \times 100\% \quad (1)$$

$$CO\ \text{selectivity}(\%) = \frac{CO_{out}}{CO_{2in} - CO_{2out}} \times 100\% \quad (2)$$

$$C_nH_m\text{selectivity}(\%) = \frac{nC_nH_m}{CO_{2in} - CO_{2out} - CO_{out}} \times 100\% \quad (3)$$

Where CO_{2in} and CO_{2out} indicate the mole amount of CO_2 at the inlet and outlet, respectively. C_nH_m represents the amounts (mole) of individual hydrocarbon products.

2.5. Characterization methods

Powder X-ray diffraction on an automated X-ray diffractometer (XRD, Rigaku Ultima IV) using Cu K-alpha radiation ($\lambda = 1.5418$ Å) was used to characterize the crystallinity of the samples. The morphology of

samples was observed using scanning electron microscopy (SEM, ZEISS SIGMA). Textural information was obtained by N_2 physisorption at 77 K on a volumetric adsorption analyzer (Micromeritics TriStar II 3020). Before the N_2 physisorption, all the samples were degassed at 200 °C for 2 h. The macropore size distribution of the samples was studied on a mercury intrusion porosimeter (Micromeritics AutoPore IV 9500). Thermal degradation behaviors of rice husks were studied on a thermogravimetric analyzer (TGA, SDT Q600). The chemical compositions of rice husk and bio-SiO_2 were studied by X-ray fluorescence spectrometry (XRF, ARL Perform X 4200) with an X-ray tube with a rhodium target (170 mA, 60 kV).

The chemical trapping experiment was carried out on temperature-programmed desorption (TPD) instrument equipped with online mass spectrometry (MS, Omnistar, Pfeiffer). Hence, the gas composition can be monitored and recorded by MS. Typically, the sample was pretreated with N_2 for 30 min at 450 °C, and then cooled down to 30 °C. The H_2/CO_2 mixture (60/20 mL/min) was introduced, and CD_3OD (with H labeled chemical trapping reagent) was introduced by using N_2 as a carrier at a flow rate of 20 mL/min at 340 °C, and the MS signals were recorded simultaneously. The MS signal of products from CO_2 hydrogenation was performed on TPD equipment combined with MS. In the CO_2 reaction, the catalysts were first pretreated with N_2 at 400 °C for 60 min before being cooled to 340 °C. Next, the H_2/CO_2 mixture (mole ratio is 3) with a flow rate of 30 mL/min was introduced to pass through the catalyst bed for CO_2 hydrogenation. The MS signals of aromatics species were recorded simultaneously.

In situ diffuse reflectance infrared Fourier transform spectroscopy (DRIFTS) was measured using an FTIR spectrometer (Thermo, Nicolet iS50) equipped with a DRIFT cell and a mercury-cadmium-telluride (MCT) detector. Before measurement, about 50 mg of the sample was pretreated at 300 °C under a 30 mL/min H_2 flow for 60 min and switched to N_2 at 300 °C for 30 min. The background was obtained after cooling down to room temperature. Subsequently, the H_2/CO_2 mixture (60/20 mL/min) was introduced to the sample cell. The information on reaction intermediates generated on the catalyst surface was recorded from room temperature to 380 °C, and the temperature was stabilized for 20 min before data collection. The DRIFT spectrometry was recorded by collecting 64 scans at 4 cm^{-1} resolution.

3. Results and discussion

3.1. Characterization of rice husk and the derived bio-SiO_2

SEM observation was employed to investigate the microstructure of pristine rice husks. Fig. 1a-c shows that rice husk exhibits a net-like fibrous microstructure with cellular struts and continuous hollow channels that form multimodal hierarchical pore structures. More importantly, the ridge-like folds are regularly arranged on the cuticles of rice husk and the cross-section of which has a bubble wrap-like framework. After calcination treatment, the naturally porous structure could be well retained (as shown in Fig. 1d-f) although the rice husk was thermally converted to bio-SiO_2. In addition, as observed in the mercury intrusion results, the macropore diameter varies from 1 to 100 μm, confirming the existence of a hierarchically porous structure of the bio-SiO_2 sample (Fig. 2a). The TEM images of bio-SiO_2 are displayed in Fig. S2, which clearly indicates that the bio-SiO_2 platform is composed of hierarchically porous thin layers with SiO_2 particles (diameter of 20–50 nm) as building blocks.

To understand the pyrolysis characteristics of rice husk, TGA analyses were carried out. As shown in Fig. 2b, the weight loss of rice husk is mainly concentrated within 550 °C, and the weight loss was 85 wt%, which is ascribed to the decomposition of the biomass (hemicellulose, cellulose, and lignin) [25]. As shown in Fig. S3, the rice husk after calcination shows a broad, intense peak assigned to amorphous silica (denoted as bio-SiO_2, herein) [31]. Rice husk is known as a Si-rich containing biomass, as it contains between 15 and 20 wt% of silica [32]. Accordingly, the rice husk with ordered, porous, and robust pore structures would be a suitable bio-platform to integrate the catalytically active components (such as metal oxides and zeolites) and fabricate bifunctional catalysts.

3.2. Characterization of $ZnZrO_x$/ZSM-5 @RH

Fig. 3 shows the synthesis process of the $ZnZrO_x$/ZSM-5 @RH bifunctional catalyst. The first step is to *in situ* immobilize $ZnZrO_x$ on the surface of rice husk (Fig. 3a) by using Schiff base-bridged MOF as precursors (*i.e.*, ZnZrMOF). In our previous work, we found that the $ZnZrO_x$ solid solution can be fabricated *via* pyrolysis of Schiff base-modified UiO-66 [30]. The H_2BDC-NH_2 organic ligand molecules are favorably coordinated with surface functional groups on the bio-template, which leads to uniformly grown ZnZrMOF octahedrons on the external surface

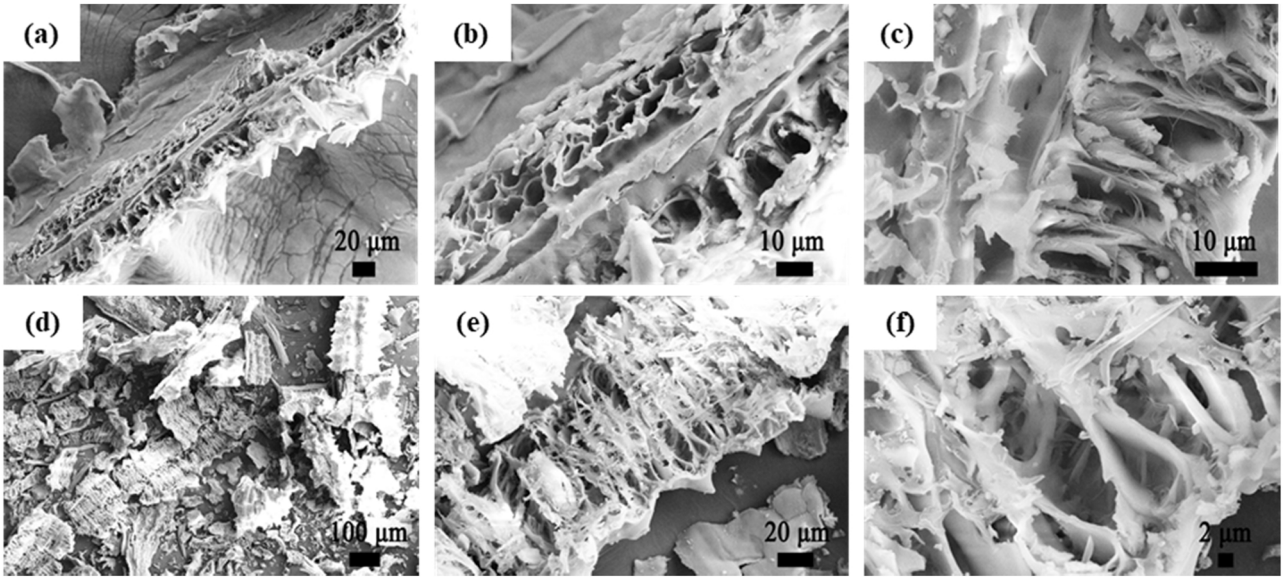

Fig. 1. SEM image of (a-c) rice husk, and (d-f) rice husk after calcination treatment (air, 550 °C), note: the calcined rice husk was named bio-SiO_2 herein.

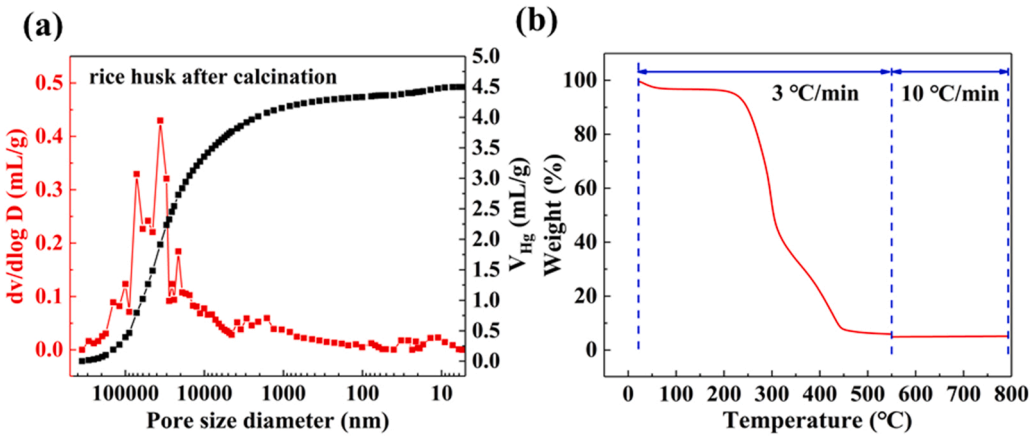

Fig. 2. (a) Cumulative intrusion (black lines) and macropore size distributions (red lines) measured by a mercury intrusion porosimeter of rice husk after calcination and (b) TGA profile of rice husk (air atmosphere).

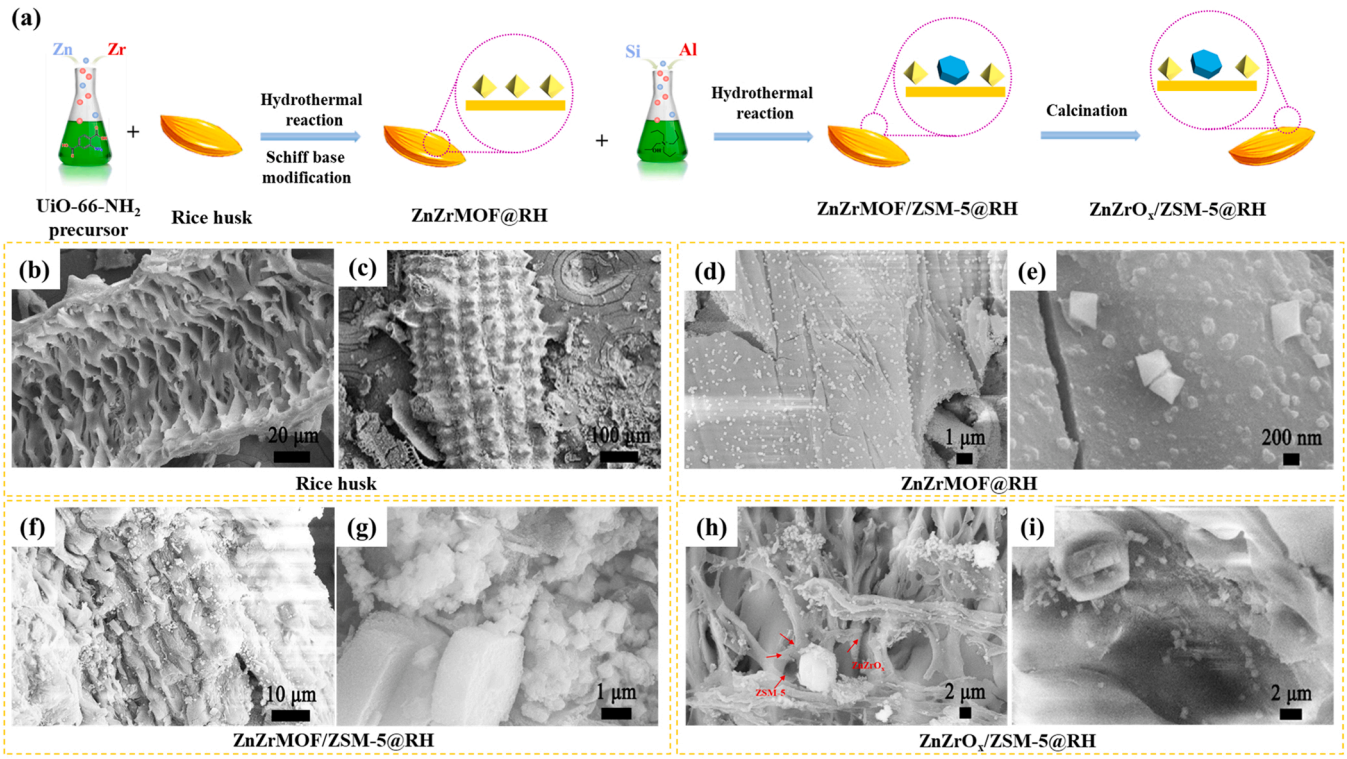

Fig. 3. (a) Schematic illustration of the preparation steps of the $ZnZrO_x$/ZSM-5 @RH bifunctional material, SEM images of (b, c) rice husk, (d, e) ZnZrMOF@RH, (f, g) ZnZrMOF/ZSM-5 @RH, and (h, i) $ZnZrO_x$/ZSM-5 @RH.

of the rice husk platform (see Fig. 3b, c).

As can be seen from the SEM images in Fig. 3d, e, the monodispersed ZnZrMOF particles (size of ~300 nm) with uniform octahedral shapes were anchored on the skeleton of the rice husk. During the subsequent hydrothermal process, the ZSM-5 particles were self-assembled in the interstitial space between ZnZrMOF particles as shown in Fig. 3f, g. After one-step calcination treatment, both $ZnZrO_x$ and ZSM-5 could be immobilized on the 3D hierarchical network of the rice husk matrix (Fig. 3h, i). As can be seen in Table S3, a higher amount of rice husks (that is, bio-SiO_2) led to lower $ZnZrO_x$/ZSM-5 content in the resulting $ZnZrO_x$/ZSM-5 @RH samples. It should be noted that the contents of K, Ca, Mn, and Fe elements are extremely low in the resulting $ZnZrO_x$/ZSM-5 @RH sample since the samples were prepared by the consecutive hydrothermal, washing, and calcination treatments (see Tables S2 and S4), which will eliminate the effect of those elements on the catalytic performance. Moreover, the residual K has little effect on the catalytic activity of the ZnZrOx/ZSM-5 catalyst, unlike the iron-based catalysts. Therefore, rice husks (or the derived bio-SiO_2) can be viewed as a suitable platform for loading $ZnZrO_x$ and ZSM-5 precursors.

3.3. *Structure and intimacy of the $ZnZrO_x$/ZSM-5 @RH*

As mentioned earlier, proper intimacy between the metallic and acidic sites guarantees the high performance of a bifunctional catalyst for CO_2 hydrogenation [33]. Numerous works have investigated the intimacy criterion over the years but are limited to synthesizing techniques in which the distance between metal and acid sites was simply tuned by varying the particle sizes of the two components [34,35]. Up to now, there are still no clear definitions to describe intimacy quantificationally. Although SEM and TEM as 2D imaging instruments have

been widely used in many areas including biological, mechanical, and materials sciences to determine the surface morphology of microscopic objects, the direct measurement of the interparticle distance by two-dimensional projection using these electron microscopies is challenging on account of the complexity of real three-dimensional supports. Hence, we resorted to Eq. 4 to estimate the average interparticle distance quantitatively by assuming the perfectly uniform particle size and equidistant distribution of particles [36]. Herein, we use the $ZnZrO_x$/ZSM-5 @RH as a model catalyst to analyze intimacy. In our synthesis, the spatial distribution of $ZnZrO_x$ and ZSM-5 was controlled by varying the amount of rice husk. For instance, a large amount of bio-SiO_2 in the $ZnZrO_x$/ZSM-5 @RH led to a far distance and low intimacy between $ZnZrO_x$ and ZSM-5, and vice versa. In other words, the bio-SiO_2 could serve as a 3D hierarchical separator, and the spatial distribution of the $ZnZrO_x$ and ZSM-5 could be controlled flexibly.

The particle size (r) and the interparticle distance (d) between metal oxides and ZSM-5 act as the quantitative descriptors of intimacy to govern the CO_2 hydrogenation ultimate product distribution. Accordingly, the intimacy is typically inversely proportional to the distance between metal oxides and zeolite (d) in two parts. For example, if the distance between metal oxides and zeolite is larger and the intimacy is small, the interparticle distance (Eq. 4) is calculated by the equation that was reported by Peng et al.[37] to quantify the critical particle distance of platinum nanoparticles. This can be done to quantify the average interparticle distance by assuming the uniform particle size, shape, and uniform distribution of $ZnZrO_x$ and ZSM-5 particles.

To corroborate the concept, we constructed $ZnZrO_x$/ZSM-5 @RH model systems by the using average interparticle distance of $ZnZrO_x$ (d_m) and ZSM-5 (d_z) to calculate the average interparticle distance of the two components (that is, $\sqrt{d_m^2 + d_z^2}$). The definitions of each parameter in the model structures of $ZnZrO_x$/ZSM-5 @RH can be found in Scheme S1. The intimacy, P, is defined as the inverse of the average interparticle distance (Eq. 5):

$$d = \sqrt{\frac{\pi}{3\sqrt{3}} \times 10^{-3} \times \rho \times \left(\frac{100 - L_M}{L_M}\right) \times A_S \times r^3} - r \tag{4}$$

$$\mathrm{P} = \frac{L}{\sqrt{d_m^2 + d_z^2}} \tag{5}$$

where ρ is the density of $ZnZrO_x$ (6.05 $g{\cdot}cm^{-3}$) or ZSM-5 (0.68 $g{\cdot}cm^{-3}$), L_M is the loading amount of $ZnZrO_x$ or ZSM-5 (wt%), A_s is the BET specific surface area of the support (rice husk after calcination, 123 $m^2{\cdot}g^{-1}$) and r (r_m and r_z) is the particle size of $ZnZrO_x$or ZSM-5. Based on our SEM observation results, the r_m (0.2 μm) was consistent in each sample, while r_z was varied in each sample, that is, 2.4, 6, 4.6, 6, and 11.4 μm as increasing the amount of rice husk. It means that ZSM-5 particles with large sizes were obtained at large amounts of rice husk. Additionally, d (d_m and d_z) is the average interparticle distance (μm) for the two components. L (2.2 mm) is the limiting distance for methanol back-mixing in the fixed-bed reactor, which is calculated by the Pe (referring to Table S5). The Pe is a class of dimensionless numbers to study the transport phenomena in a continuum. Pe is defined as the ratio of the advection rate to the diffusion rate of the same quantity driven by concentration gradients. Generally, if the Pe number is smaller than 1, the diffusion rate dominates over the advection rate [38]. Thus, the Pe number can be used to assess "how far the methanol reaction intermediate can diffuse upstream against the CO_2/H_2 feed gas flow" [21]. By considering all the parameters that may affect the Pe number, a distance of 2.2 mm was obtained when assuming that the Pe number was 1 (referring to Table S5). Accordingly, the intimacy (the dimensionless number P) of the MO&ZEO catalyst can be presented as the ratio of L (2.2 mm) to the mean of d_m and d_z.

As illustrated in Fig. 4, d value (d_m and d_z) stands for the interparticle distance of the neighboring $ZnZrO_x$ and ZSM-5 active sites on the MO&ZEO catalysts. As expected, both increasing the rice husk amount

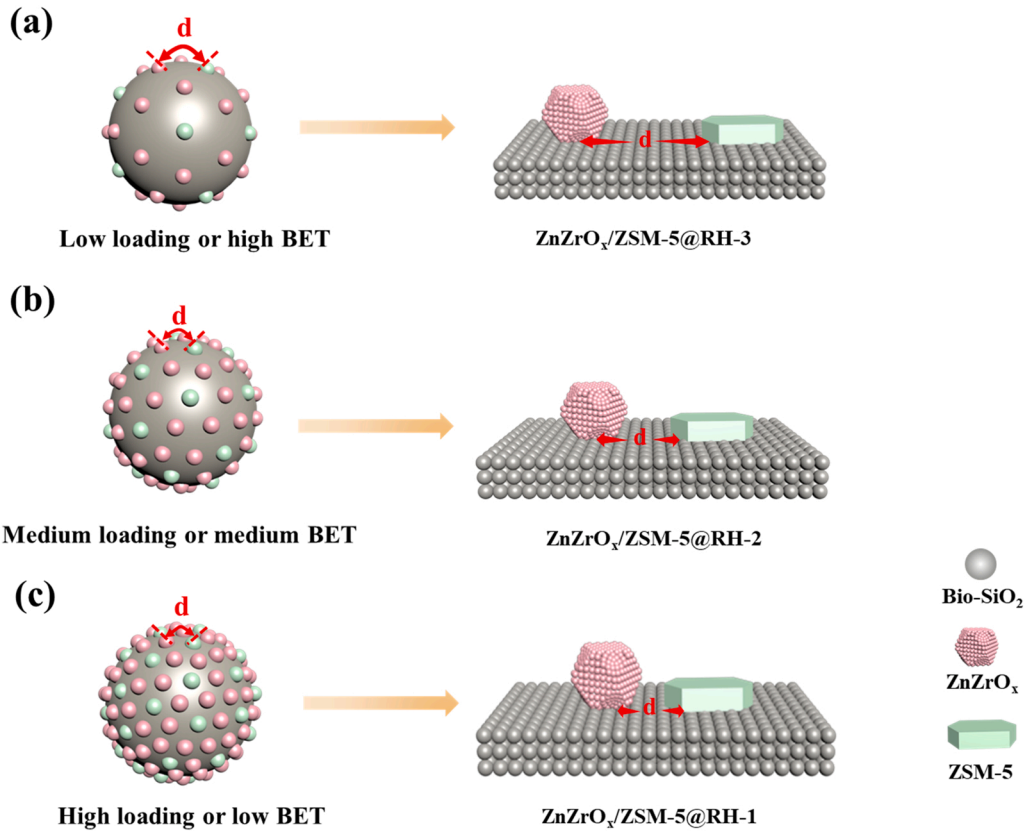

Fig. 4. Schematic illustration of the bifunctional $ZnZrO_x$/ZSM-5 @RH with varying intimacy using bio-SiO_2 as a platform (or separator). (a) Using a high amount of rice husk or high surface area supports results in lower MO&ZEO loading with a much larger interparticle distance, (b) shortening the distance between $ZnZrO_x$ and ZSM-5 particles by decreasing the rice husk amount to 2 g or medium surface area support, and (c) further strengthening the intimacy between $ZnZrO_x$ and ZSM-5 by using 1 g of rice husk or low surface area supports.

(L_M↓) or using higher surface area support (A_S↑) can enlarge the interparticle distance (d↑), and vice versa. To quantitatively calculate the intimacy between the metal oxide and zeolite, five different $ZnZrO_x$/ZSM-5 @RH catalysts prepared by varying the amount of rice husk were constructed, including $ZnZrO_x$/ZSM-5 @RH-1 (60.1 wt% of $ZnZrO_x$/ZSM-5), $ZnZrO_x$/ZSM-5 @RH-1.5 (42 wt% of $ZnZrO_x$/ZSM-5), $ZnZrO_x$/ZSM-5 @RH-2 (20 wt% of $ZnZrO_x$/ZSM-5), $ZnZrO_x$/ZSM-5 @RH-2.5 (14 wt% of $ZnZrO_x$/ZSM-5), and $ZnZrO_x$/ZSM-5 @RH-3 (12 wt% of $ZnZrO_x$/ZSM-5). The $ZnZrO_x$/ZSM-5 @RH-1 had the closest intimacy between octahedral $ZnZrO_x$ and the ZSM-5 particles and the d value (*i.e.*, $\sqrt{d_m^2 + d_z^2}$) was calculated to be 1.1 μm according to Eqs. (4) and (5). By increasing the bio-template amount of rice husk to 1.5–3 g, more separator was introduced and the mean d values (average interdistance) of $ZnZrO_x$/ZSM-5 @RH-1.5, $ZnZrO_x$/ZSM-5 @RH-2, $ZnZrO_x$/ZSM-5 @RH-2.5, and $ZnZrO_x$/ZSM-5 @RH-3 were increased to 1.3, 2.06, 6.05, and 22.87 μm, respectively.

TEM images of obtained bifunctional catalysts are shown in Fig. S4, but it can not determine the interparticle distance of the two components. As can be seen in Fig. 5, SEM images compare the spatial configuration of the octahedral $ZnZrO_x$ and coffin-like ZSM-5 on the bifunctional catalysts. When the addition amount of rice husk was only 1 g, the $ZnZrO_x$ and ZSM-5 particles tended to be located close to each other. As shown in Fig. 5a, the prepared $ZnZrO_x$/ZSM-5 @RH-1 exhibited high intimacy of $ZnZrO_x$ and ZSM-5. Hence, the $ZnZrO_x$/ZSM-5 @RH-1 demonstrated the closest intimacy between octahedral $ZnZrO_x$ and the ZSM-5 particles, and the P value was calculated to be 1940 according to Eq. (5). By increasing the bio-template amount of rice husk from 1.5 g to 3 g, the higher amount of bio-SiO_2 separator was introduced. As a result, the mean P value was decreased to 1681, 1069, 363, and 96, respectively, when increasing the amount of rice husk.

In most current literature, MO and ZEO composite catalysts are typically made by physical mixing methods (*e.g.*, dual bed, granule mixing, powder mixing), which leads to a random distribution of MO particles on the ZEO particles. Therefore, the MO-catalyzed and ZEO-catalyzed reactions may occur in parallel order rather than in tandem order. In comparison, the three-dimensional rice husk and the derived bio-SiO_2 platform provide three-dimension multiscale networks to assemble MO and ZEO components with controlled intimacy. In particular, we found that intimacy can also be tuned flexibly by changing the amount of rice husk (Scheme S2).

The XRD pattern of bio-ZSM-5 (Fig. S5) showed the characteristic diffraction peaks at 7.97°, 8.91°, 23.3°, 23.7°, and 24.5°, belonging to the typical MFI structure. While the broad diffraction peak between 20° and 25° can be assigned to the bio-SiO_2 platform. Moreover, the XRD pattern of $ZnZrO_x$ solid solutions (Fig. S6) prepared by using MOFs as precursors exhibited characteristic diffraction peaks at $2\theta = 30.5°$, 50.1°, and 60° due to tetragonal ZrO_2 (JCPDS No. 50–1089), indicating the formation of solid solution structure [28]. Furthermore, XRD characterization showed that all the $ZnZrO_x$/ZSM-5 @RH catalysts processed both tetragonal $ZnZrO_x$ solid solution structure and ZSM-5 classic MFI structure (Fig. 6a), showing that both $ZnZrO_x$ and ZSM-5 phases coexist in the composite [39]. In comparison to $ZnZrO_x$/ZSM-5 @RH-3, the $ZnZrO_x$/ZSM-5 @RH-1 processed stronger crystallization degrees, which is attributed to the $ZnZrO_x$/ZSM-5 @RH-1 containing relatively higher loading contents of the two components. Whereas, the $ZnZrO_x$/ZSM-5 @RH-3 contained significant cristobalite SiO_2 species (PDF#77–1317) due to high Si content in rice husk [40]. Moreover, N_2 physisorption measurements showed that the specific BET surface areas of $ZnZrO_x$/ZSM-5 @RH-1, $ZnZrO_x$/ZSM-5 @RH-2, and $ZnZrO_x$/ZSM-5 @RH-3 catalysts were 313, 257, and 230 m^2/g, respectively, and the pore volumes were 0.518, 0.382, and 0.310 cm^3/g, respectively. As displayed in Table S6 and Fig. S7, the pore size distributions based on Barrett-Joyner-Halenda (BJH) method suggest the average mesopore size of $ZnZrO_x$/ZSM-5 @RH-1, $ZnZrO_x$/ZSM-5 @RH-2, and $ZnZrO_x$/ZSM-5 @RH-3 samples were 6, 6, and 8 nm, respectively. The mesopore volume (V_{meso}) and surface area (S_{meso}) of the three catalysts were 0.31, 0.38, 0.52 $cm^3 \cdot g^{-1}$ and 101.7, 111.2, 185.3 $m^2 \cdot g^{-1}$, respectively. Combined with the SEM observations in Fig. 5 and S8, it can be safely confirmed that $ZnZrO_x$/ZSM-5 @RH-3 indeed owned hierarchical porosity induced by the bio-SiO_2. It was found that $ZnZrO_x$/ZSM-5 @RH-3 exhibited the largest values of mesopore volume and mesopore surface area due to more rice husks being added. Moreover, the bio-ZSM-5 had decreased amount of Brønsted acid

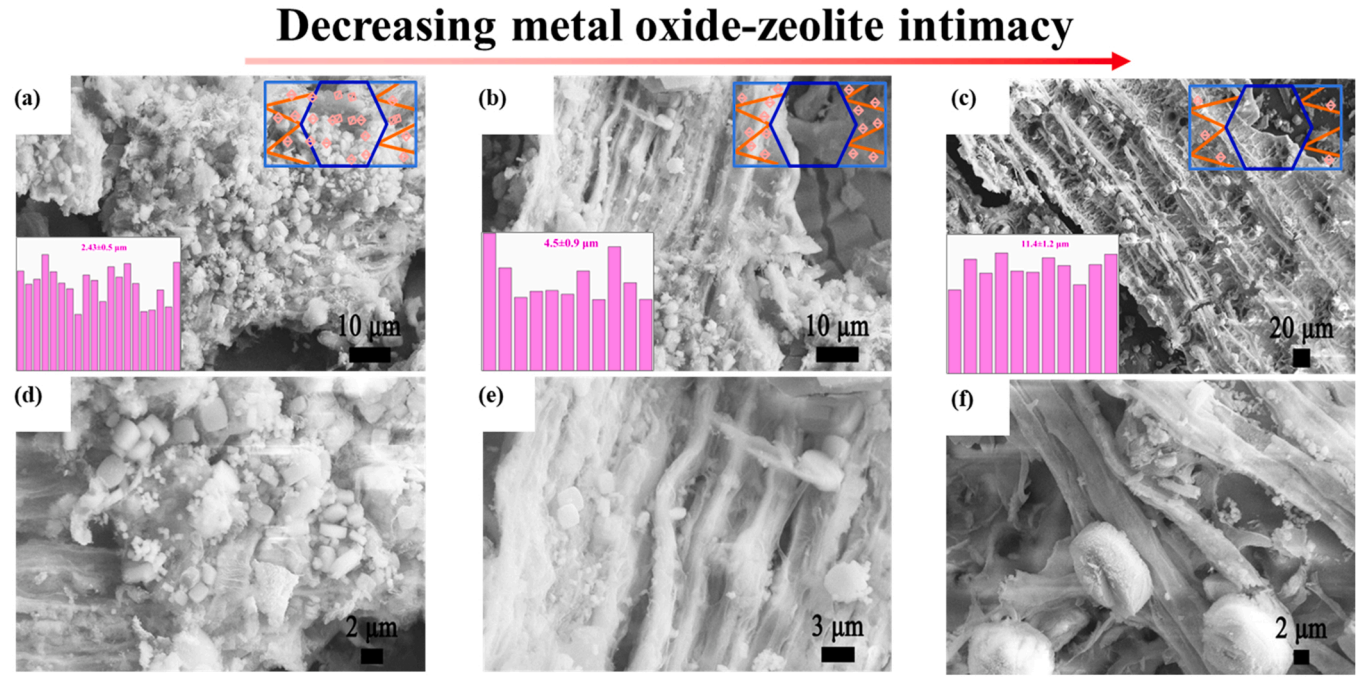

Fig. 5. Representative SEM images of $ZnZrO_x$/ZSM-5 @RH with varying intimacy of metal oxide and zeolite, (a, d) $ZnZrO_x$/ZSM-5 @RH-1, (b, e) $ZnZrO_x$/ZSM-5 @RH-2, and (c, f) $ZnZrO_x$/ZSM-5 @RH-3. The insects in (a-c) represent the model of $ZnZrO_x$/ZSM-5 @RH with different intimacy and the histograms of particle size distributions of ZSM-5 and the histograms of the particle size distribution of ZSM-5.

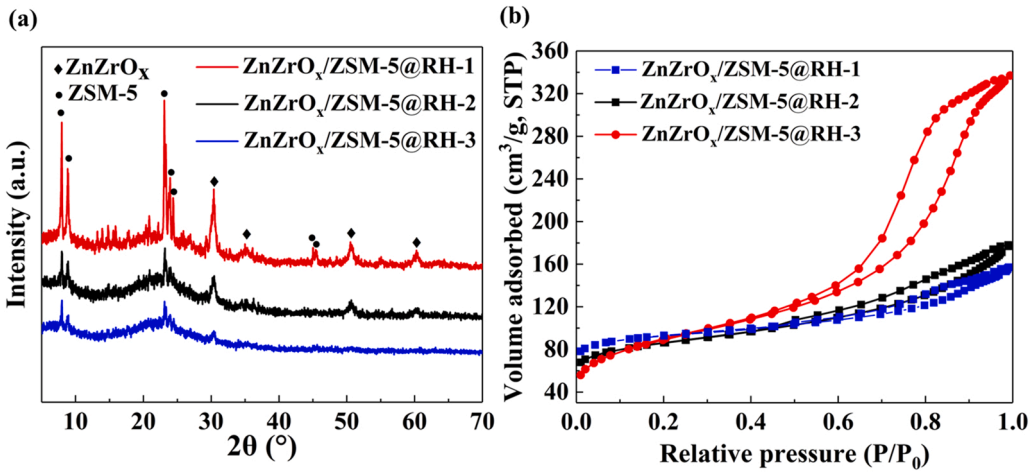

Fig. 6. (a) XRD patterns (b) N_2 physisorption isotherms of $ZnZrO_x$/ZSM-5 @RH integrated catalysts with different intimacy using bio-SiO_2 as a platform (or separator).

sites as compared to the traditional ZSM-5 without adding rice husk [18], which is due to the formation of distorted frameworks of Al species.

3.4. CO_2 hydrogenation performance of $ZnZrO_x$/ZSM-5 @RH

To investigate the effect of intimacy between $ZnZrO_x$ and ZSM-5 on the CO_2 hydrogenation performance, the obtained $ZnZrO_x$/ZSM-5 @RH bifunctional catalysts with different specific intimacy were further applied to the selective conversion of CO_2 to aromatics tandem reaction (Fig. 7a). In detail, with decreasing the intimacy between $ZnZrO_x$ and ZSM-5 zeolite, the CO_2 conversion of $ZnZrO_x$/ZSM-5 @RH-3, $ZnZrO_x$/ZSM-5 @RH-2.5, $ZnZrO_x$/ZSM-5 @RH-2, $ZnZrO_x$/ZSM-5 @RH-1.5, $ZnZrO_x$/ZSM-5 @RH-1 was 6.8%, 8.5%, 12.2%, 12%, and 12.1%, respectively. Meanwhile, the aromatics selectivity was 26.2%, 54%, 74.7%, 70%, and 69.1%, respectively. On the other hand, the corresponding CH_4 selectivity was 5.6%, 4.2%, 1.1%, 2.1%, and 2%, respectively. So, the proximity of metal oxide and zeolite should play a vital role in the catalytic performance of the CO_2 hydrogenation tandem process.

With the larger distance between the metal oxide and zeolite, lower CO_2 conversion (6.8%) and aromatics selectivity (26.2%) were obtained for the $ZnZrO_x$/ZSM-5 @RH-3 catalyst (Fig. 7a, mode d). It may be ascribed to the excessive separation of the $ZnZrO_x$ and ZSM-5 particles, and the communication between $ZnZrO_x$ and ZSM-5 *via* methanol intermediate is insufficient enough to drive CO_2 conversion over $ZnZrO_x$. Thus, the C_2^0-C_4^0 alkanes formed from over-hydrogenation became favorable and the aromatization and isomerization reactions were

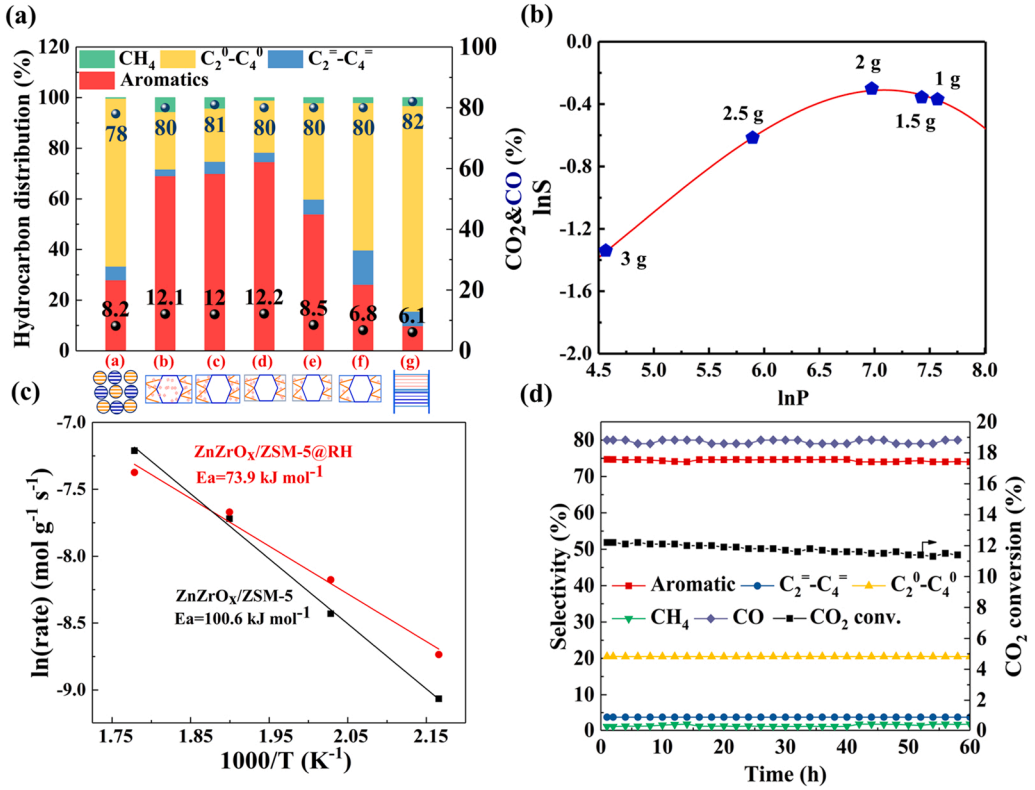

Fig. 7. Catalytic performance of $ZnZrO_x$/ZSM-5 @RH bifunctional with different intimacy in CO_2 hydrogenation to aromatics. (a) CO_2 conversion, CO selectivity, and products distribution of hydrocarbons (mode a: physical mixing, mode b-f: integration manner with adding different amounts of rice husk, mode g: dual bed configuration), (b) stimulated relationship curve between aromatic selectivity and intimacy of the bifunctional catalysts, (c) Arrhenius plots of $ZnZrO_x$/ZSM-5 @RH and $ZnZrO_x$/ZSM-5 fabricated by powder mixing for methanol synthesis (reaction conditions: H_2/CO_2 =3:1; P = 3 MPa; F=30 mL/min), and (d) long-term stability test of $ZnZrO_x$/ZSM-5 @RH-2 catalyst towards CO_2 hydrogenation during 60 h on stream.

restricted. The closer distance between metal and acid functions in $ZnZrO_x$/ZSM-5 @RH-2 showed that the CO_2 conversion was increased almost double (12.2% *vs.* 6.8%), and the products shifted to aromatics (Fig. 7a, mode c, 74.7%). The CO_2 conversion over $ZnZrO_x$/ZSM-5 @RH-2 was increased as the consumption of methanol on ZSM-5 downstream could greatly drive the CO_2 conversion over $ZnZrO_x$. This enhancement in intimacy could remarkably reduce the methanol intermediate diffusion distance and increase the local concentration of methanol for subsequent reaction on ZSM-5 zeolite [21]. In addition, no methanol was detected, suggesting that the methanol could always be converted to other products over the acid sites downstream. By arranging the $ZnZrO_x$ and ZSM-5 at a close distance, the aromatics selectivity was 69.1% at CO_2 conversion of 12.1% (Fig. 7a, mode b). Moreover, we also eliminated the effect of particle sizes and porosity of biomass templates on the catalytic performance. It is hard to keep the porosity the same for all the samples with different intimacy. However, in our previous work [18], the bio-ZSM-5 prepared by using the rice husk or luffa sponge as biotemplates led to a similar catalytic activity of CO_2 hydrogenation to DME due to the hierarchical porous structures. As shown in Fig. S9, the $ZnZrO_x$ (300, 100, and 50 nm) and ZSM-5 (4500, 550, and 300 nm) with different sizes have been synthesized. The CO_2 hydrogenation to CH_3OH over $ZnZrO_x$ with different sizes is shown in Fig. S9g. No obvious difference was observed due to the Zn concentration in the $ZnZrO_x$ solid solution playing a vital role [30]. We further physically mixed the $ZnZrO_x$ and ZSM-5 and investigated the CO_2 hydrogenation to aromatic activity. The results indicated that all the samples yielded the same aromatics selectivity and CO_2 conversion (Fig. S9h), probably due to that the physical mixing method led to fixed proximity. In comparison, the rice husk derived-SiO_2 was employed as a platform to tune the proximity, which can be adjusted by changing the amount of biomass during the catalyst fabrication.

To investigate the intimacy effect, previous studies controlled the distance between two components by varying the configuration manner, such as dual-bed, stacking of granules with sizes simple mixing of the two components in an agate mortar. Wang et al. found that increasing the intimacy of two components can increase the aromatics selectivity, but further increasing the intimacy to certain content, the aromatics selectivity increased slightly [28]. Whereas, further increasing the intimacy might cause deactivation due to the migration of metals to zeolite driven by the harsh reaction condition [17]. So, $ZnZrO_x$/ZSM-5 @RH-1 and $ZnZrO_x$/ZSM-5 @RH-2 with close intimacy exhibited similar catalytic activity.

The aromatic hydrocarbon distribution for CO_2 hydrogenation over $ZnZrO_x$/ZSM-5 @RH catalyst was further analyzed. As can be seen in Fig. S10, the main byproducts were trimethylbenzene, xylene, and tetramethylbenzene. Specifically, the selectivity of 1,2,4-trimethylbenzene was 27.63%, 1,3,5-trimethylbenzene was 9.97%, xylene was 32.97% (o-xylene 14.86%, m-xylene & p-xylene 18.11%), and tetramethylbenzene was 18.79%. Considering that the steric effects of H-ZSM-5 restrict the formation of aromatic hydrocarbons larger than 1,2,4-trimethylbenzene, the formation of heavier aromatics should be due to the alkylation reactions on zeolite surfaces.

Furthermore, NH_3-TPD profiles of the three $ZnZrO_x$/ZSM-5 @RH catalysts were quite similar (Fig. S11). The NH_3 desorption peak of the three $ZnZrO_x$/ZSM-5 @RH bifunctional catalysts appeared at low temperatures of 100–200 °C, medium temperatures of 250–400 °C, and high temperatures of 500–600 °C, which can be ascribed to physical adsorption, medium and strong acid sites of bio-ZSM-5. The peak areas of $ZnZrO_x$/ZSM-5 @RH-1 were much stronger than $ZnZrO_x$/ZSM-5 @RH-2 and $ZnZrO_x$/ZSM-5 @RH-3. The reason can be attributed to the higher loading amount of $ZnZrO_x$ and ZSM-5 leading to the increased moderate and strong acid sites. When $ZnZrO_x$ and bio-ZSM-5 were integrated with high intimacy (*viz.*, $ZnZrO_x$/ZSM-5 @RH-1), the NH_3 desorption peak at low and medium temperature shifted to a lower temperature compared with that of $ZnZrO_x$/ZSM-5 @RH-2 and $ZnZrO_x$/ZSM-5 @RH-3, which is due to the synergy effect (such as migration of metals to zeolite driven by high temperature) between the acidic zeolite site and $ZnZrO_x$.

However, by physical mixing (the powdery $ZnZrO_x$ and the ZSM-5 were initially pressed, crushed, and sieved into 40–60 mesh granules, then simply mixed by shaking in a vessel), the aromatics selectivity and CO_2 conversion were only 28% and 8.2%, respectively (Fig. 7a, mode a). This was much lower as compared to that of $ZnZrO_x$/ZSM-5 @RH-1, with aromatics selectivity and CO_2 conversion of 69.1% and 12.1%, respectively. We found that the separation of the two separate components by the quartz wool forming dual bed configuration method (Fig. 7a, mode e) has not only decreased the CO_2 conversion (6.1%) because of the lack of thermodynamic driving force but also decreased the aromatics selectivity to only 9.9%. The light olefins became the main products due to the longer contact time required for the products formed on $ZnZrO_x$ to be further converted to aromatics over downstream sites of ZSM-5. Apparently, the tandem reaction efficiency is sensitive to the distance between the two components.

Therefore, in this study, we try to explore an empirical equation to describe the intimacy effect by adjusting the model catalysts with a specific arrangement. The empirical equations predict the relationship between aromatic selectivity S and the intimacy of two components. We constructed $ZnZrO_x$/ZSM-5 @RH model systems by calculating interparticle distances of $ZnZrO_x$ (d_m) and ZSM-5 (d_z) separately. The models' predictive ability was verified by the experimental data. To determine whether there is a quantitative relationship between the intimacy and the selectivity of aromatics, the dimensionless number *P* of the bifunctional catalysts is plotted as a function of aromatics selectivity (Fig. 7b). A high correlation between the *P* value and aromatics selectivity of $ZnZrO_x$/ZSM-5 @RH integrated catalysts has been uncovered, which indicates a strong correlation to the intimacy between $ZnZrO_x$ and ZSM-5. Herein, Eq. (6) was used to simulate the relationship between the intimacy *P* of the bifunctional catalysts and the selectivity of aromatics (*S*) in CO_2 hydrogenation. The dependence of *P* and *S* is revealed by further fitted by Eq. (6), giving an R^2 value of 0.9994, whereby, the dimensionless number *P* represents the intimacy value, and *S* represents the selectivity of aromatics, respectively (referring to Fig. 7b). This further confirms that the aromatics selectivity in CO_2 hydrogenation reactions is greatly relevant to the intimacy between the metal oxides and zeolite of bifunctional catalysts.

$$\ln(S) = -0.03827 \times (\ln P - 0.3098) \times (\ln P - 7.081)^2 - 0.3098 \quad (6)$$

These results demonstrate that the spatial arrangement between $ZnZrO_x$ and ZSM-5 particles can significantly affect the selectivity of aromatics. Therefore, the formation of aromatics is strongly depending on the synergy effect between the $ZnZrO_x$ and ZSM-5 components. The aromatics selectivity increased with an increase in the intimacy of the two components, suggesting the formation of the aromatics is due to the efficient synergy between the $ZnZrO_x$ and ZSM-5. However, there should be optimal intimacy for maximizing aromatic selectivity. The too-close intimacy between the two components probably led to the unfavorable over-hydrogenation of the aromatics.

The apparent activation energy (E_a) is a well-known empirical parameter in chemical kinetics that characterizes the dependence of the reaction rate coefficients on the temperature, which also shed light on the intrinsic activity of the catalysts [41]. Thus, the apparent activation energy for methanol synthesis for $ZnZrO_x$/ZSM-5 @RH integrated catalyst and $ZnZrO_x$/ZSM-5 was calculated as the reactions were conducted at relatively lower temperatures (below 300 °C). As can be seen, the activation energy of methanol synthesis of $ZnZrO_x$/ZSM-5 @RH integrated catalyst is 73.9 kJ•mol^{-1}, which is obviously lower than that of $ZnZrO_x$/ZSM-5 with physical mixing (E_a=100.6 kJ•mol^{-1}). Therefore, lower E_a of the methanol synthesis could boost the generation of a higher amount of intermediates for the tandem reaction, which further demonstrates the superiority of the integrated bifunctional catalyst by using bio-SiO_2 as a platform.

Furthermore, long-term stability is critical to its industrial application. The zeolite catalyzes the MTA reaction because of its unique topology and acidic property, but a high density of acid sites and small pore size may accelerate the catalyst deactivation due to coke deposition and serious channel blockage [42]. As can be seen from Fig. 7d, $ZnZrO_x$/ZSM-5 @RH catalyst was tested for 60 h on stream, which showed excellent catalytic stability. The selectivity of aromatics and CO_2 conversion was maintained at around 74% and 12%, respectively, during the entire period. In addition, no obvious crystalline structure/morphology changes were found in the spent $ZnZrO_x$/ZSM-5 @RH catalyst as confirmed by the XRD patterns (Fig. S12) and the SEM image (Fig. S13), suggesting the high stability of the designed integrated catalyst.

3.5. Proposed reaction mechanisms

To further investigate the reaction mechanism of the CO_2 hydrogenation over the $ZnZrO_x$/ZSM-5 @RH catalyst, the reaction intermediates were detected by *in situ* DRIFT spectra (Fig. 8a). Under the reaction condition, the IR bands centered at 2976 cm^{-1}, 2888 cm^{-1}, and 2738 cm^{-1} belonging to *HCOO species were observed [39]. The IR bands centered at 2935 cm^{-1} and 2824 cm^{-1} can be attributed to the $*CH_3O$ [28]. Therefore, the $ZnZrO_x$ catalyst probably followed the formate-methoxy reaction pathway for the methanol formation *via* CO_2 hydrogenation, which is consistent with the reaction mechanism proposed by other reported Zr-based catalysts [43]. Unlike the pure $ZnZrO_x$, as the $ZnZrO_x$ was integrated with ZSM-5, it was found that the intensities of the IR bands at 2935 and 2824 cm^{-1} belonging to the absorbed $*CH_3O$ species decreased (Fig. 8b) [44]. This implied that the $*CH_3O$ species transferred to the ZSM-5 (having the acid sites) for further cyclization and aromatization reaction.

Moreover, chemical trapping is another convenient technology to identify the reaction intermediates [29]. $CO_2/H_2/CD_3OD$ (the hydrogen was labeled) isotope-switching studies were carried out using mass spectrometry. The CD_3OD was used as a trapping agent to react with the $*CH_3O$ and *HCOO reaction intermediates and to verify the intermediate formation. As can be seen in Fig. 8c, after switching to $CO_2/H_2/C$-D_3OD, the mass signal assigned to CD_3OCH_3, CD_3CHO derived from $*CH_3O$, *CHO, and $HCOOCD_3$ derived from *HCOO were detected, respectively [29]. Afterward, when CD_3OD was cut off, the signal of CD_3OCH_3, CD_3CHO, and $HCOOCD_3$ disappeared, indicating that both $*CH_3O$ and *HCOO species were the main reaction intermediates produced on $ZnZrO_x$ sites.

Furthermore, as shown in Fig. 8d-f, the formation time for aromatics products (*e.g.*, C_8H_{10}, C_9H_{12}, and $C_{10}H_{14}$) over $ZnZrO_x$/ZSM-5 @RH catalysts with different intimacy was compared, which reflects the C-C bond coupling and aromatization ability of the tandem catalyst under reaction conditions ($CO_2 + H_2$). The reaction process over $ZnZrO_x$/ZSM-5 @RH-2 (22 min) with dimensionless number *P* of 1069 was much faster than that of $ZnZrO_x$/ZSM-5 @RH-1 (40 min) and $ZnZrO_x$/ZSM-5 @RH-3 (59 min) with *P* values of 1940 and 96, respectively. The results were consistent with the catalytic performance in Fig. 7a. It should be noted that the aromatics were produced *via* oligomerization of higher linear alkenes catalyzed by the acidic sites on ZSM-5, followed by isomerization, aromatization, and cracking. This result affirmed that appropriate intimacy between the metal oxide and zeolite assures a whole journey of a dual-cycle for the conversion of methanol over ZSM-5 (MTA process, see Fig. S14) [45].

4. Conclusion

Typically, the intimacy of the bifunctional catalyst for CO_2 hydrogenation is adjusted by using different configuration methods, such as dual-bed configuration, powder physical mixing, granule stacking, or ball-milling [46]. Herein, we developed a new method to study the effect of the intimacy of $ZnZrO_x$ and ZSM-5 on the catalytic performance of CO_2 hydrogenation to aromatics. Particularly, we proposed a new configuration of MO&ZEO catalysts by using rice husk (the derived

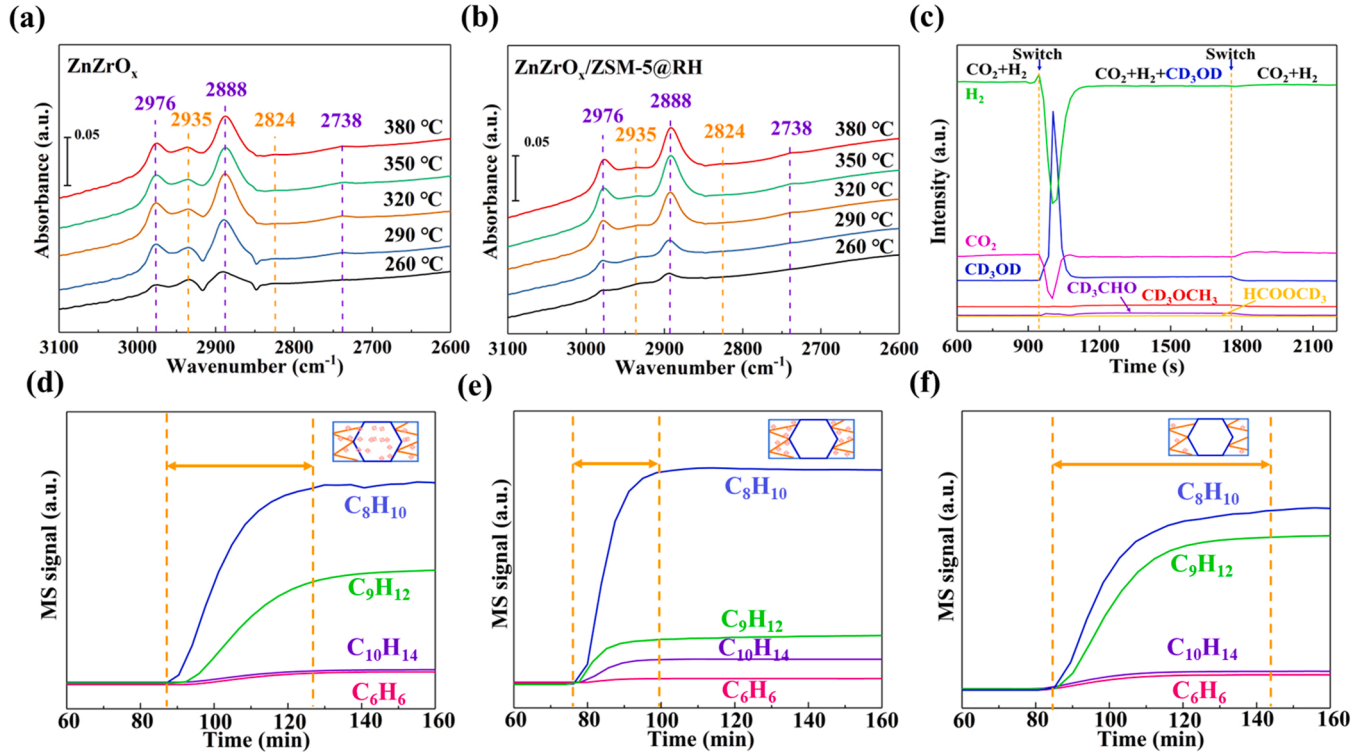

Fig. 8. *In situ* DRIFT spectra of (a) the $ZnZrO_x$ and (b) $ZnZrO_x$/ZSM-5 @RH in the CO_2 hydrogenation atmosphere. (c) Chemical trapping MS spectra with CD_3OD trapping reagent over $ZnZrO_x$ for CO_2 hydrogenation. MS spectra of N_2 subsequently switched to CO_2 and H_2 over (d) $ZnZrO_x$/ZSM-5 @RH-1, (e) $ZnZrO_x$/ZSM-5 @RH-2, and (f) $ZnZrO_x$/ZSM-5 @RH-3.

bio-SiO_2) to immobilize metal oxide and zeolite components, which is quite different from the conventional physical mixing method for the fabrication of bifunctional MO&ZEO catalysts. In total, five $ZnZrO_x$/ZSM-5 @RH integrated catalysts with different intimacy have been prepared and used to investigate the intimacy-dependent selectivity of CO_2 hydrogenation to aromatics. The rice husk and the derived hierarchically porous bio-SiO_2 was employed as the bio-platform (or separator) to integrate $ZnZrO_x$ and ZSM-5 with accurate intimacy. The distance between the metal oxide and zeolites was preliminarily quantified highly depending on the amount of rice husk. It was found that the combination of $ZnZrO_x$ with ZSM-5 to form the $ZnZrO_x$/ZSM-5 @RH integrated catalyst has effectively improved the selectivity for aromatics products from 28% (physical mixing) to 74.7%, which also showed good long-term stability. *In situ* DRIFTS and chemical trapping results revealed that close contact between bifunctional sites benefited the conversion of *HCOO and *CH_3O intermediates to higher alkenes followed by isomerization, aromatization, and cracking on the ZSM-5 acidic sites, resulting in the generation of aromatics with high selectivity. In addition, the preliminary relationship between intimacy and aromatics selectivity was uncovered, which might open an avenue for the integration of multiple active sites with controlled spatial configuration and suitable intimacy for tandem catalysis reactions.

CRediT authorship contribution statement

Wen Li: Writing – original draft, Methodology, Data curation. **Guowu Zhan:** Conceptualization, Supervision, Writing – review & editing. **Xiaobin Liu:** Data curation. **Yihua Yue:** Data curation. **Kok Bing Tan:** Writing – review & editing. **Jia Wang:** Methodology. **Jiale Huang:** Conceptualization, Supervision. **Qingbiao Li:** Supervision.

Declaration of Competing Interest

The authors declare that they have no known competing financial interests or personal relationships that could have appeared to influence the work reported in this paper.

Data availability

Data will be made available on request.

Acknowledgments

This work was supported by the National Natural Science Foundation of China (Nos. U21A20324 and 22278167), the Natural Science Foundation of Fujian Province (Nos. 2022J01115 and 2021J06026), the Education and Research Foundation of the Ministry of Education of Fujian Province for Young Teachers (No. JAT210015), and the Technology Innovation Center for Exploitation of Marine Biological Resources, MNR (No. TICMBR202204).

Appendix A. Supporting information

Supplementary data associated with this article can be found in the online version at doi:10.1016/j.apcatb.2023.122575.

References

[1] J. Zhong, X. Yang, Z. Wu, B. Liang, Y. Huang, T. Zhang, State of the art and perspectives in heterogeneous catalysis of CO_2 hydrogenation to methanol, Chem. Soc. Rev. 49 (2020) 1385–1413.
[2] W. Li, K. Wang, G. Zhan, J. Huang, Q. Li, Design and synthesis of bioinspired $ZnZrO_x$&bio-ZSM-5 integrated nanocatalysts to boost CO_2 hydrogenation to light olefins, ACS Sustain. Chem. Eng. 9 (2021) 6446–6458.
[3] P.S. Rezaei, H. Shafaghat, W.M.A.W. Daud, Production of green aromatics and olefins by catalytic cracking of oxygenate compounds derived from biomass pyrolysis: A review, Appl. Catal. a-Gen. 469 (2014) 490–511.
[4] Y.M. Ni, Z.Y. Chen, Y. Fu, Y. Liu, W.L. Zhu, Z.M. Liu, Selective conversion of CO_2 and H_2 into aromatics, Nat. Commun. 9 (2018) 1–7.
[5] R.-P. Ye, J. Ding, W. Gong, M.D. Argyle, Q. Zhong, Y. Wang, C.K. Russell, Z. Xu, A. G. Russell, Q. Li, M. Fan, Y.-G. Yao, CO_2 hydrogenation to high-value products via heterogeneous catalysis, Nat. Commun. 10 (2019) 5698.
[6] D. Wang, Z. Xie, M.D. Porosoff, J.G. Chen, Recent advances in carbon dioxide hydrogenation to produce olefins and aromatics, Chem 7 (2021) 2277–2311.
[7] C. Pei, J. Gong, Tandem catalysis at nanoscale, Science 371 (2021) 1203–1204.
[8] H. Choi, S. Oh, S.B. Trung Tran, J.Y. Park, Size-controlled model Ni catalysts on Ga_2O_3 for CO_2 hydrogenation to methanol, J. Catal. 376 (2019) 68–76.
[9] S. De, A. Dokania, A. Ramirez, J. Gascon, Advances in the design of heterogeneous catalysts and thermocatalytic processes for CO_2 utilization, ACS Catal. 10 (2020) 14147–14185.
[10] G. Devender, G. Rimzhim, M.-G. Raghu, P.S. C., Review of catalyst design and mechanistic studies for the production of olefins from anthropogenic CO_2, ACS Catal. 10 (2020) 14258–14282.
[11] J. Sun, C. Mu, D. Guo, Y. Zhao, S. Wang, X. Ma, Effects of intimacy between acid and metal sites on the isomerization of n-C16 at the large/minor nanoscale and atomic scale, ACS Catal. 12 (2022) 4092–4102.
[12] M. Wang, Z. Wang, S. Liu, R. Gao, K. Cheng, L. Zhang, G. Zhang, X. Min, J. Kang, Q. Zhang, Y. Wang, Synthesis of hierarchical SAPO-34 to improve the catalytic performance of bifunctional catalysts for syngas-to-olefins reactions, J. Catal. 394 (2021) 181–192.
[13] K. Cheng, B. Gu, X. Liu, J. Kang, Q. Zhang, Y. Wang, Direct and highly selective conversion of synthesis gas into lower olefins: design of a bifunctional catalyst combining methanol synthesis and carbon-carbon coupling, Angew. Chem. Int. Ed. 55 (2016) 4725–4728.
[14] Y. Wang, W. Zhan, Z. Chen, J. Chen, X. Li, Y. Li, Advanced 3D hollow-out ZnZrO@C combined with hierarchical zeolite for highly active and selective CO hydrogenation to aromatics, ACS Catal. 10 (2020) 7177–7187.
[15] N. Li, B. Huang, X. Dong, J. Luo, Y. Wang, H. Wang, D. Miao, Y. Pan, F. Jiao, J. Xiao, Z. Qu, Bifunctional zeolites-silver catalyst enabled tandem oxidation of formaldehyde at low temperatures, Nat. Commun. 13 (2022) 2209.
[16] Q. Zhang, J. Yu, A. Corma, Applications of zeolites to C1 chemistry: recent advances, challenges, and opportunities, Adv. Mater. 2002927 (2020) 1–31.
[17] Y. Wang, G. Wang, L.I. van der Wal, K. Cheng, Q. Zhang, K.P. de Jong, Y. Wang, Visualizing element migration over bifunctional metal-zeolite catalysts and its impact on catalysis, Angew. Chem. Int. Ed. 60 (2021) 17735–17743.
[18] W. Li, K. Wang, G. Zhan, J. Huang, Q. Li, Hydrogenation of CO_2 to dimethyl ether over tandem catalysts based on biotemplated hierarchical ZSM-5 and Pd/ZnO, ACS Sustain. Chem. Eng. 8 (2020) 14058–14070.
[19] P.B. Weisz, Polyfunctional heterogeneous catalysis, Adv. Catal. 13 (1962) 137–190.
[20] J. Zecevic, G. Vanbutsele, K.P. de Jong, J.A. Martens, Nanoscale intimacy in bifunctional catalysts for selective conversion of hydrocarbons, Nature 528 (2015) 245–254.
[21] Y. Li, M. Wang, S. Liu, F. Wu, Q. Zhang, S. Zhang, K. Cheng, Y. Wang, Distance for communication between metal and acid sites for syngas conversion, ACS Catal. 12 (2022) 8793–8801.
[22] X. Jiang, Y. Liu, H.J. Hao, Y. Xu, J.L. Huang, D.H. Sun, Q.B. Li, Rape pollen-templated synthesis of C,N self-doped hierarchical TiO_2 for selective hydrogenation of 1,3-butadiene, ACS Sustain. Chem. Eng. 6 (2018) 882–888.
[23] X. Liu, G. Zhan, J. Wu, W. Li, Z. Du, J. Huang, D. Sun, Q. Li, Preparation of integrated CuO/ZnO/OS nanocatalysts by using acid-etched oyster shells as a support for CO_2 hydrogenation, ACS Sustain. Chem. Eng. 8 (2020) 7162–7173.
[24] W.-T. Tsai, Y.-Q. Lin, H.-J. Huang, Valorization of Rice Husk for the Production of Porous Biochar, Mater., Ferment. 7 (2021) 70.
[25] Z. Chen, X. Wang, B. Xue, W. Li, Z. Ding, X. Yang, J. Qiu, Z. Wang, Rice husk-based hierarchical porous carbon for high performance supercapacitors: The structure-performance relationship, Carbon 161 (2020) 432–444.
[26] P. Tian, G. Zhan, J. Tian, K.B. Tan, M. Guo, Y. Han, T. Fu, J. Huang, Q. Li, Direct CO_2 hydrogenation to light olefins over $ZnZrO_x$ mixed with hierarchically hollow SAPO-34 with rice husk as green silicon source and template, Appl. Catal. B: Environ. 315 (2022), 121572.
[27] J.J. Wang, G.N. Li, Z.L. Li, C.Z. Tang, Z.C. Feng, H.Y. An, H.L. Liu, T.F. Liu, C. Li, A highly selective and stable ZnO-ZrO_2 solid solution catalyst for CO_2 hydrogenation to methanol, Sci. Advanves 3 (2017) 1–10.
[28] C. Zhou, J. Shi, W. Zhou, K. Cheng, Q. Zhang, J. Kang, Y. Wang, Highly active ZnO-ZrO_2 aerogels integrated with H-ZSM-5 for aromatics synthesis from carbon dioxide, ACS Catal. 10 (2020) 302–310.
[29] Z. Li, Y. Qu, J. Wang, H. Liu, M. Li, S. Miao, C. Li, Highly selective conversion of carbon dioxide to aromatics over tandem catalysts, Joule (2019) 1–14.
[30] W. Li, K. Wang, J. Huang, X. Liu, D. Fu, J. Huang, Q. Li, G. Zhan, M_xO_y-ZrO_2 (M = Zn, Co, Cu) solid solutions derived from schiff base-bridged UiO-66 composites as high-performance catalysts for CO_2 hydrogenation, ACS Appl. Mater. Interfaces 11 (2019) 33263–33272.
[31] M.K. Rybarczyk, Y. Li, M. Qiao, Y.-S. Hu, M.-M. Titirici, M. Lieder, Hard carbon derived from rice husk as low cost negative electrodes in Na-ion batteries, J. Energy Chem. 29 (2019) 17–22.
[32] K. Fujisawa, Y. Lei, C. de Tomas, I. Suarez-Martinez, C.J. Zhou, Y.C. Lin, S. Subramanian, A.L. Elias, M. Fujishige, K. Takeuchi, J.A. Robinson, N.A. Marks, M. Endo, M. Terrones, Facile 1D graphene fiber synthesis from an agricultural by-product: A silicon-mediated graphenization route, Carbon 142 (2019) 78–88.
[33] Impact of the spatial organization of bifunctional metal–zeolite catalysts on the hydroisomerization of light alkanes, Angew. Chem. Int. Ed., 132 (2020) 3620–3628.

[34] D. Xu, H. Yang, X. Hong, G. Liu, S.C. Edman, Tsang, Tandem catalysis of direct CO_2 hydrogenation to higher alcohols, ACS Catal. (2021) 8978–8984.
[35] K. Cheng, W. Zhou, J. Kang, S. He, S. Shi, Q. Zhang, Y. Pan, W. Wen, Y. Wang, Bifunctional catalysts for one-step conversion of syngas into aromatics with excellent slectivity and sability, Chem 3 (2017) 334–347.
[36] J.C. Meier, C. Galeano, I. Katsounaros, J. Witte, H.J. Bongard, A.A. Topalov, C. Baldizzone, S. Mezzavilla, F. Schüth, K.J. Mayrhofer, Design criteria for stable Pt/C fuel cell catalysts, Beilstein J. Nanotechnol. 5 (2014) 44–67.
[37] P. Yin, S. Hu, K. Qian, Z. Wei, L.-L. Zhang, Y. Lin, W. Huang, H. Xiong, W.-X. Li, H.-W. Liang, Quantification of critical particle distance for mitigating catalyst sintering, Nat. Commun. 12 (2021) 4865.
[38] M. Huysmans, A. Dassargues, Review of the use of Péclet numbers to determine the relative importance of advection and diffusion in low permeability environments, Hydrogeol. J. 13 (2005) 895–904.
[39] J.J. Wang, G.N. Li, Z.L. Li, C.Z. Tang, Z.C. Feng, H.Y. An, H.L. Liu, T.F. Liu, C. Li, A highly selective and stable ZnO-ZrO_2 solid solution catalyst for CO_2 hydrogenation to methanol, Sci. Adv. 3 (2017) 1–10.
[40] D. Ding, S. Yang, X. Qian, L. Chen, T. Cai, Nitrogen-doping positively whilst sulfur-doping negatively affect the catalytic activity of biochar for the degradation of organic contaminant, Appl. Catal. B: Environ. 263 (2020), 118348.
[41] L. Chen, Z. Qi, X. Peng, J.-L. Chen, C.-W. Pao, X. Zhang, C. Dun, M. Young, D. Prendergast, J.J. Urban, J. Guo, G.A. Somorjai, J. Su, Insights into the mechanism of methanol steam reforming tandem reaction over CeO_2 supported single-site catalysts, J. Am. Chem. Soc. 143 (2021) 12074–12081.
[42] M. Wang, J. Kang, X. Xiong, F. Zhang, K. Cheng, Q. Zhang, Y. Wang, Effect of zeolite topology on the hydrocarbon distribution over bifunctional ZnAlO/SAPO catalysts in syngas conversion, Catal. Today 371 (2021) 85–92.
[43] J. Wang, C. Tang, G. Li, Z. Han, Z. Li, H. Liu, F. Cheng, C. Li, High performance $MaZrO_x$ (Ma=Cd, Ga) solid solution catalysts for CO_2 hydrogenation to methanol, ACS Catal. (2019) 10253–10259.
[44] J. Zuo, W. Chen, J. Liu, X. Duan, L. Ye, Y. Yuan, Selective methylation of toluene using CO_2 and H_2 to para-xylene, Sci. Adv. 6 (2020) 1–8.
[45] U. Olsbye, S. Svelle, M. Bjorgen, P. Beato, T.V.W. Janssens, F. Joensen, S. Bordiga, K.P. Lillerud, Conversion of methanol to hydrocarbons: how zeolite cavity and pore size controls product selectivity, Angew. Chem. Int. Ed. 51 (2012) 5810–5831.
[46] W. Zhou, K. Cheng, J. Kang, C. Zhou, V. Subramanian, Q. Zhang, Y. Wang, New horizon in C1 chemistry: breaking the selectivity limitation in transformation of syngas and hydrogenation of CO_2 into hydrocarbon chemicals and fuels, Chem. Soc. Rev. 48 (2019) 3193–3228.